

---

This is an electronic reprint of the original article.  
This reprint may differ from the original in pagination and typographic detail.

Dai, Yunyun; Wang, Yadong; Das, Susobhan; Li, Shisheng; Xue, Hui; Mohsen, Ahmadi; Sun, Zhipei

## Broadband Plasmon-Enhanced Four-Wave Mixing in Monolayer MoS<sub>2</sub>

*Published in:*  
Nano Letters

*DOI:*  
[10.1021/acs.nanolett.1c02381](https://doi.org/10.1021/acs.nanolett.1c02381)

Published: 28/07/2021

*Document Version*  
Publisher's PDF, also known as Version of record

*Published under the following license:*  
CC BY

*Please cite the original version:*  
Dai, Y., Wang, Y., Das, S., Li, S., Xue, H., Mohsen, A., & Sun, Z. (2021). Broadband Plasmon-Enhanced Four-Wave Mixing in Monolayer MoS<sub>2</sub>. *Nano Letters*, 21(14), 6321-6327.  
<https://doi.org/10.1021/acs.nanolett.1c02381>

---

This material is protected by copyright and other intellectual property rights, and duplication or sale of all or part of any of the repository collections is not permitted, except that material may be duplicated by you for your research use or educational purposes in electronic or print form. You must obtain permission for any other use. Electronic or print copies may not be offered, whether for sale or otherwise to anyone who is not an authorised user.

# Broadband Plasmon-Enhanced Four-Wave Mixing in Monolayer MoS<sub>2</sub>

Yunyun Dai,\* Yadong Wang, Susobhan Das, Shisheng Li, Hui Xue, Ahmadi Mohsen, and Zhipei Sun\*



Cite This: *Nano Lett.* 2021, 21, 6321–6327



Read Online

ACCESS |



Metrics & More



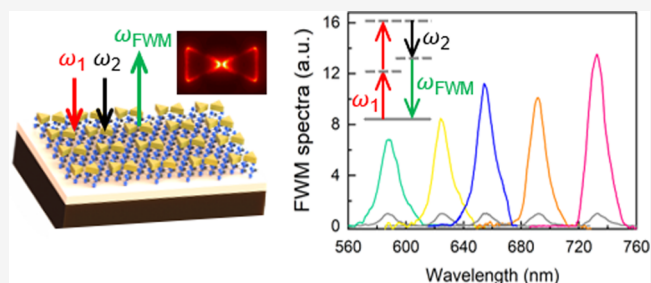
Article Recommendations



Supporting Information

**ABSTRACT:** Two-dimensional transition-metal dichalcogenide monolayers have remarkably large optical nonlinearity. However, the nonlinear optical conversion efficiency in monolayer transition-metal dichalcogenides is typically low due to small light–matter interaction length at the atomic thickness, which significantly obstructs their applications. Here, for the first time, we report broadband (up to  $\sim 150$  nm) enhancement of optical nonlinearity in monolayer MoS<sub>2</sub> with plasmonic structures. Substantial enhancement of four-wave mixing is demonstrated with the enhancement factor up to three orders of magnitude for broadband frequency conversion, covering the major visible spectral region. The equivalent third-order nonlinearity of the hybrid MoS<sub>2</sub>-plasmonic structure is in the order of  $10^{-17}$  m<sup>2</sup>/V<sup>2</sup>, far superior ( $\sim 10$ – $100$ -times larger) to the widely used conventional bulk materials (e.g., LiNbO<sub>3</sub>, BBO) and nanomaterials (e.g., gold nanofilms). Such a considerable and broadband enhancement arises from the strongly confined electric field in the plasmonic structure, promising for numerous nonlinear photonic applications of two-dimensional materials.

**KEYWORDS:** Two-dimensional materials, nonlinear optics, four-wave mixing, plasmonic enhancement, MoS<sub>2</sub>



Nonlinear optics in the nanoscale regime has attracted massive attention in the last decades.<sup>1</sup> For example, it provides a host of fascinating phenomena (e.g., saturable absorption),<sup>2</sup> which are remarkably useful for photonic applications such as ultrafast pulse generation.<sup>3–5</sup> Among various nonlinear optical processes, four-wave mixing (FWM), a third-order optical nonlinear process, plays a key role for a large range of applications (such as frequency conversion, signal amplification, and optical switching).<sup>6,7</sup> Recently, two-dimensional (2D) transition-metal dichalcogenides (TMDs)<sup>8</sup> have attracted tremendous interest due to their unique physical properties, such as strong excitonic effect,<sup>9,10</sup> dynamic electrical tunability,<sup>11,12</sup> and large optical nonlinearity.<sup>13–22</sup> As newly emerging nanoscale nonlinear materials, TMDs exhibit fascinating optical nonlinearity such as the excitonic enhancement of harmonic generation.<sup>19,23</sup> Especially, recently the gate-tunable second-harmonic generation (SHG)<sup>24</sup> and FWM<sup>25</sup> have been realized in TMDs.<sup>26</sup> All these results show the great potential of using TMDs for diverse on-chip nonlinear optical devices, fundamentally different from those based on traditional bulk materials.<sup>1,25</sup>

However, the applications of TMDs in nonlinear optics are limited due to the low conversion efficiency caused by the short light–matter interaction length at their atomic thickness. Several approaches have been proposed including plasmonics,<sup>27–30</sup> photonic cavities,<sup>31</sup> and waveguide integration.<sup>32</sup> Among them, plasmonics provides an excellent platform for enhancing light–matter interaction, which shows great

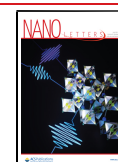
potential for nanoscale nonlinear optical applications.<sup>33–37</sup> For example, the SHG of WS<sub>2</sub> on the silver nanogroove grating was enhanced by the plasmonic resonance, with a large enhancement factor ( $\sim 400$ ).<sup>33</sup> Besides, SHG of bilayer WSe<sub>2</sub> was obtained by the plasmonic hot carrier injection.<sup>38</sup> Nevertheless, plasmonic enhancement of FWM in TMDs has not been studied yet and deserves further investigation.

Here, for the first time, we report broadband FWM enhancement in monolayer MoS<sub>2</sub> with plasmonic structures. An enhancement factor up to three orders of magnitude is achieved compared to the FWM generated from bare MoS<sub>2</sub> monolayer without plasmonic structures. The massive enhancement is attributed to the strongly confined electric field of the pump light in the hot spots of the plasmonic structures. The FWM enhancement with different excitation polarization states and plasmonic structure dimensions is also investigated. Furthermore, for the first time, we demonstrate a broadband (up to  $\sim 150$  nm) enhancement of FWM in the hybrid MoS<sub>2</sub>-plasmonic structure with an in-depth discussion about the broadband enhancement mechanism. The plasmon-

**Received:** June 18, 2021

**Revised:** July 12, 2021

**Published:** July 19, 2021



induced significant and broadband FWM enhancement in 2D materials is promising for numerous applications in the future nonlinear photonics.

**Results and Discussion.** *MoS<sub>2</sub>-Plasmonic Nanostructures.* A schematic layout and an optical image of the hybrid MoS<sub>2</sub>-plasmonic structure are shown in Figure 1a and b.

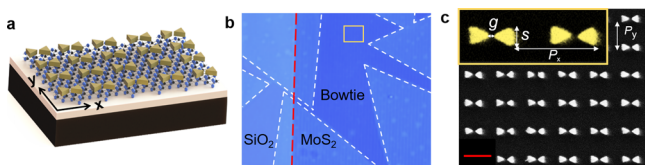


**Figure 1.** Hybrid MoS<sub>2</sub>-plasmonic nanostructures. (a) Schematic illustration and (b) optical image of the MoS<sub>2</sub>-plasmonic structure (Au bowtie) on a SiO<sub>2</sub>/Si substrate. In the optical image, the white dashed lines outline the edges of the MoS<sub>2</sub> flakes, and the red dashed line outlines the boundary of the plasmonic nanostructures and the bare SiO<sub>2</sub>/Si substrate. (c) SEM image of the Au bowtie nanostructures. Scale bar: 500 nm. Inset: zoomed image of Au bowtie nanostructures. Structure parameters are also labeled.

Monolayer MoS<sub>2</sub> flakes grown on a SiO<sub>2</sub>/Si substrate by the chemical vapor deposition (CVD) method<sup>39</sup> are of the triangular shape and appear lighter colored compared to the substrate. By examining Raman and photoluminescence spectra (Figure S1, Supporting Information), the CVD MoS<sub>2</sub> flakes are identified as monolayers. The 50 nm-thick gold nanostructures are then patterned on top of the MoS<sub>2</sub> flakes (fabrication details in the Supporting Information). The scanning electron microscopy (SEM) image of a typical Au bowtie array is shown in Figure 1c. The size of each equilateral

triangle ( $s$ ) is  $\sim 160$  nm, and the gap ( $g$ ) is  $\sim 30$  nm, with the unit cell pitch  $P_x = P_y = \sim 600$  nm.

*Plasmon Enhanced FWM in Monolayer MoS<sub>2</sub>.* An illustration of the FWM process in the hybrid MoS<sub>2</sub>-plasmonic structure is shown in Figure 2a. The MoS<sub>2</sub> sample, excited by pump and idler beams with frequencies at  $\omega_1$  and  $\omega_2$  ( $\omega_1 > \omega_2$ ), generates FWM signals at  $\omega_{\text{FWM}} = 2\omega_1 - \omega_2$ , following the law of conservation of energy. The lower panel in Figure 2a shows the energy level diagram of the FWM process. To measure the FWM signals, a home-built femtosecond laser based microscopic setup (Figure 2b) is employed. The input pump and idler laser beams are linearly polarized with polarizations parallel along the  $x$ -axis. For other polarizations (e.g., the pump and idler beams are cross-polarized), they are fully discussed in Figure S3 of the Supporting Information. The pump and idler beams are spatially merged using a dichroic mirror and are temporally synchronized by a delay line. The combined beams are focused on the sample through an objective lens. The generated nonlinear optical signals in the MoS<sub>2</sub> sample are measured in a reflection configuration by a spectrometer.

Here, we use a pump photon energy ( $\hbar\omega_1$ ) at  $\sim 1.55$  eV ( $\lambda_1 = \sim 800$  nm) and an idler photon energy ( $\hbar\omega_2$ ) at  $\sim 1.19$  eV ( $\lambda_2 = \sim 1040$  nm). Then the generated FWM photon energy ( $\omega_{\text{FWM}} = 2\omega_1 - \omega_2$ ) is at  $\sim 1.91$  eV ( $\lambda_{\text{FWM}} = \sim 650$  nm). In the experiment, the average powers for both pump and idler input light are fixed as  $\sim 1$   $\mu\text{W}$  (with a corresponding peak intensity of  $\sim 44$  GW/cm<sup>2</sup>) unless otherwise specified. The plasmonic structures are fabricated on one portion of a few MoS<sub>2</sub> monolayer flakes (Figure 1b), which allows for a self-consistent comparison of FWM from the same MoS<sub>2</sub> flake with and without plasmonic structures. As shown in Figure 2c, the FWM peak intensity measured from the MoS<sub>2</sub>-plasmonic structures is

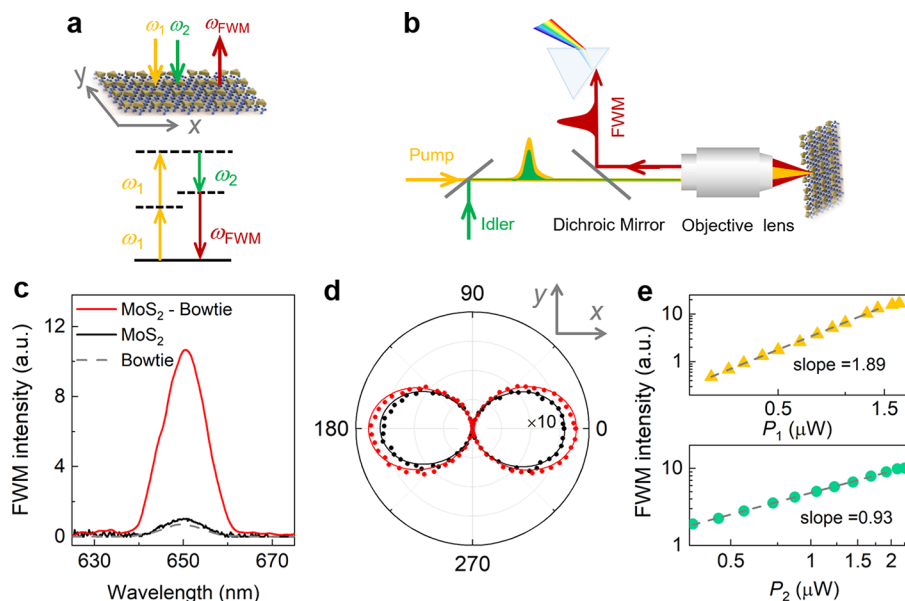


**Figure 2.** Plasmon-enhanced FWM in monolayer MoS<sub>2</sub>. (a) Illustration of FWM from the hybrid MoS<sub>2</sub>-plasmonic structures (upper panel) and the energy level diagram of FWM process (lower panel). (b) Schematic of the experimental setup for nonlinear optical measurements. (c) FWM spectra measured from hybrid MoS<sub>2</sub>-plasmonic structures (red curve), bare MoS<sub>2</sub> monolayer without plasmonic structure (black curve), and the plasmonic structure only (gray dashed curve). (d) Generated FWM signals from the hybrid MoS<sub>2</sub>-plasmonic structures (red) and the bare MoS<sub>2</sub> monolayer (black) through a polarization analyzer are plotted as a function of angle  $\theta$  between the polarization analyzer axis and the  $x$ -axis. The experiment data (dots) can be well fitted by a  $\cos^2 \theta$  curve. (e) Dependence of experimental FWM peak intensities on the average power of the pump ( $P_1$ ) and probe light ( $P_2$ ), with a fit to a power law  $I^m$ . Upper panel: Dependence of FWM on  $P_1$  with a fit ( $m = \sim 1.89$ ). Lower panel: Dependence of FWM on  $P_2$  with a fit ( $m = \sim 0.93$ ).

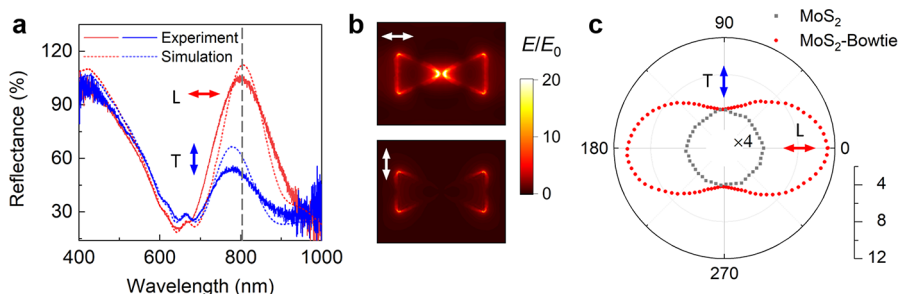


**Figure 3.** FWM polarization dependence. (a) Experimental (solid curves) and simulated (dotted curves) reflection spectra, (b) simulated electric field at 800 nm at different input polarizations (upper, the longitudinal mode; lower, the transverse mode). (c) Experimental FWM intensity from bare MoS<sub>2</sub> (gray dots) and hybrid MoS<sub>2</sub>-plasmonic structure (red dots) as a function of polarization angle  $\alpha$  between the polarization of incident beams and the  $x$ -axis.

one order of magnitude ( $\sim 11$ -fold) higher than that from the bare MoS<sub>2</sub> region (i.e., without the plasmonic structure) and the pristine bowtie plasmonic structure. The results fully demonstrate the significant plasmonic enhancement of the third-order optical nonlinearity in 2D materials. Apart from FWM, there also exist multiple nonlinear optical processes in the hybrid MoS<sub>2</sub>-plasmon nanostructures. Figure S4 in the Supporting Information presents the spectra of the multiple nonlinear processes (e.g., SHG, Sum frequency generation, and FWM) on bare MoS<sub>2</sub> and hybrid MoS<sub>2</sub>-plasmon nanostructures.

The polarization of the generated FWM signal is also measured. Here, both the pump and idler beams are linearly polarized along the  $x$ -axis, and a polarization analyzer for the generated FWM signal is set at an angle  $\theta$  with respect to the  $x$ -axis. Figure 2d presents the FWM versus  $\theta$  taken on bare MoS<sub>2</sub> monolayer (i.e., without plasmonic structures) and the hybrid MoS<sub>2</sub>-plasmonic structures, respectively. The observed FWM signals from both the bare MoS<sub>2</sub> and the hybrid MoS<sub>2</sub>-plasmonic structures are linearly polarized along the  $x$ -axis, fitted well by  $\cos^2 \theta$ , agreeing well with the previous experimental FWM results.<sup>22</sup>

The power dependence of the generated FWM signal from the hybrid MoS<sub>2</sub>-plasmonic structures is examined by changing the pump power  $P_1$  and the idler power  $P_2$ , respectively. The upper panel of Figure 2e shows the peak intensities of the FWM as a function of  $P_1$  in a log–log scale, while  $P_2 = \sim 1 \mu\text{W}$ . The lower panel of Figure 2e shows the peak intensities of FWM spectra as a function of  $P_2$  on a log–log scale, while  $P_1 = \sim 1 \mu\text{W}$ . It roughly follows a square and linear power-law behavior as a function of the pump power and idler power, respectively, which confirms the detected signal is generated by the FWM process when excited by the pump and idler beams. Note that it gets slightly saturated at high pump/idler powers possibly due to the intrinsic loss (e.g., multiphoton absorption) of the pump light and FWM signals,<sup>40</sup> and the shift of the plasmonic resonance (e.g., shape deformation of the nanostructure) at high incidence power.<sup>41</sup>

For a quantitative comparison, the experimental enhancement factor ( $EF_{\text{ex}}$ ) for FWM in the hybrid MoS<sub>2</sub>-plasmonic structure is calculated from the results shown in Figure 2c. Considering that the hot spot of the plasmonic structure (i.e., the gap of the Au bowtie nanostructure) uniformly occupies a small area in the array, the  $EF_{\text{ex}}$  can be approximately calculated as<sup>42</sup>

$$EF_{\text{ex}} = \frac{I_{\text{MoS}_2\text{-bowtie}}}{I_{\text{MoS}_2}} \frac{A_0}{A_{\text{gap}}} \quad (1)$$

where  $I_{\text{MoS}_2\text{-bowtie}}$  and  $I_{\text{MoS}_2}$  are the measured FWM intensities from MoS<sub>2</sub> with and without the bowtie plasmonic structure,  $A_0$  represents the area of the unit cell in this array, and  $A_{\text{gap}}$  represents the hot spot area of the plasmonic structure (i.e., the gap of the bowtie nanostructure). Accounting for the small hot spot area fraction ( $A_{\text{gap}}/A_0 = \sim 0.25\%$ ) and  $\sim 11$ -fold FWM enhancement ( $\frac{I_{\text{MoS}_2\text{-bowtie}}}{I_{\text{MoS}_2}}$ ) from the hybrid MoS<sub>2</sub>-plasmonic structures, the estimated maximum  $EF_{\text{ex}}$  at the plasmonic hot spot is calculated to be  $\sim 4400$  for the incident beam polarized along the  $x$ -axis shown in Figure 2. In addition, we also estimate the theoretical enhancement factor ( $EF_{\text{th}}$ ) of  $\sim 5250$  (details in the Supporting Information), which agrees with our experimental results. Therefore, the plasmonic resonance strongly enhances the light–matter interactions in 2D materials, and the enhancement factor up to three orders of magnitude is achieved.

**FWM Enhancement with Different Polarizations.** The bowtie nanostructures typically support different plasmonic modes along with  $x$  and  $y$  directions. When the incident light is linearly polarized along the  $x$ -axis, the longitudinal plasmonic modes are excited. While the incident light is linearly polarized along the  $y$ -axis, the transverse plasmonic modes are excited. Here, we study the polarization dependence of the hybrid MoS<sub>2</sub>-plasmonic structure. The experimental reflection spectra of the hybrid MoS<sub>2</sub>-plasmonic structure on the SiO<sub>2</sub>/Si substrate are measured with  $x$  and  $y$  polarizations, agreeing well with the simulated reflection spectra, as shown in Figure 3a. The relative reflection spectra ( $R = R_{\text{MoS}_2\text{-bowtie}}/R_{\text{sub}}$ ) feature broad peaks for both polarizations, where  $R_{\text{MoS}_2\text{-bowtie}}$  is the reflection from the hybrid MoS<sub>2</sub>-plasmonic structures and  $R_{\text{sub}}$  is the reflection from a bare SiO<sub>2</sub>/Si substrate. Note that the small peaks at around 620 and 660 nm are the B- and A-excitonic states of MoS<sub>2</sub>, clearly observed both in the experimental and simulated spectra. The significant peaks in the reflection spectra are attributed to the longitudinal and transverse plasmonic resonances, as confirmed by simulated electric field enhancement in the bowtie nanostructures at the wavelength of 800 nm (Figure 3b). The detailed simulations are introduced in Figure S5 in the Supporting Information. The longitudinal plasmonic resonance ( $\hbar\omega_{p_L}$ ) is at  $\sim 1.55$  eV ( $\lambda_{p_L} = \sim 800$  nm), while the transverse plasmonic resonance is at a slightly higher energy  $\hbar\omega_{p_T} = 1.63$  eV ( $\lambda_{p_T} = \sim 760$  nm).

For transverse mode, no interaction between the two neighboring triangular nanostructures is observed (the lower panel in Figure 3b), which corresponds to the dark spot in the gap. In contrast, for the longitudinal mode, the plasmonic modes supported by two neighboring triangular structures within one bowtie structure are strongly coupled, leading to the relative redshift of the longitudinal plasmonic mode.<sup>43</sup> The hot spot inside the gap of the bowtie structure as illustrated in the upper panel of Figure 3b is an evidence for this strong interaction. We observe that the electric field enhancement with the longitudinal mode within the plasmonic structure (i.e., the gap of the bowtie) is much stronger than that of the transverse mode where the electric field is only enhanced along the two sides of the bowtie.<sup>44</sup>

The longitudinal and transverse plasmonic modes have totally different resonances (e.g., resonant wavelengths, electric fields), resulting in different enhancement behaviors in the nonlinear optical process. Here, we study the angular dependence of the FWM enhancement in the hybrid MoS<sub>2</sub>-plasmonic structure. Figure 3c shows the experimental FWM peak intensity measured from monolayer MoS<sub>2</sub> with and without the plasmonic structure as a function of the polarization angle  $\alpha$  between the incident beams and the  $x$ -axis. Note that the pump and idler beams are linearly polarized with polarizations parallel with each other. The details of the measurement setup are shown in Figure S6a in the Supporting Information. In contrast to the isotropic FWM from bare MoS<sub>2</sub>, the FWM intensity from the hybrid MoS<sub>2</sub>-plasmonic structure varies with  $\alpha$ . When the pump laser is polarized along the  $x$ -axis ( $\alpha = 0^\circ$ ), it is resonant with the longitudinal plasmonic mode at the wavelength of 800 nm, the FWM enhancement reaches the maximum ( $\sim 11$ -fold), higher than that from the transverse mode ( $\sim 4$ -fold) with the  $y$ -axis polarized excitation ( $\alpha = 90^\circ$ ). The spectra of the enhanced FWM signals at  $\alpha = 0^\circ$  and  $90^\circ$  are shown in Figure S6b in the Supporting Information. Between the two critical angles where is a superposition of two plasmonic modes, the enhancement of the nonlinear optical process varies between the maximum to the minimum. Therefore, tuning the polarization of the pump laser enables the modulation of the plasmons in the nanostructures, thus tuning the FWM intensity of the hybrid MoS<sub>2</sub>-plasmonic structure.

**FWM Enhancement with Different Plasmonic Structure Dimensions.** To further understand the plasmon-enhanced FWM process, we fabricate Au bowtie nanostructures with different dimensions on top of monolayer MoS<sub>2</sub>. The SEM images of the patterned Au bowties are shown in the left panel of Figure 4a, with structure size  $s$  varying from 160 to 120 nm, while the gap ( $g = 30$  nm) and the pitch ( $P_x = P_y = 600$  nm) are fixed. The simulated electric field for the longitudinal polarization at 800 nm is presented in the right panel of Figure 4a. Figure 4b presents the experimental relative reflection spectra ( $R = R_{\text{MoS}_2\text{-bowtie}}/R_{\text{sub}}$ ) measured from the Au nanostructure arrays on monolayer MoS<sub>2</sub> with the longitudinal polarization, agreeing well with the simulated reflection spectra. Details of the simulated reflection spectra are shown in Figure S5 in the Supporting Information. The plasmon resonance shows the redshift from 740 to 800 nm with the increment of the structure size  $s$ . The strengths of the plasmonic resonance, shown as the amplitude of the reflection peaks, are stronger with the increasing structure size, which fits well with the simulation results of the electric field in Figure 4a.

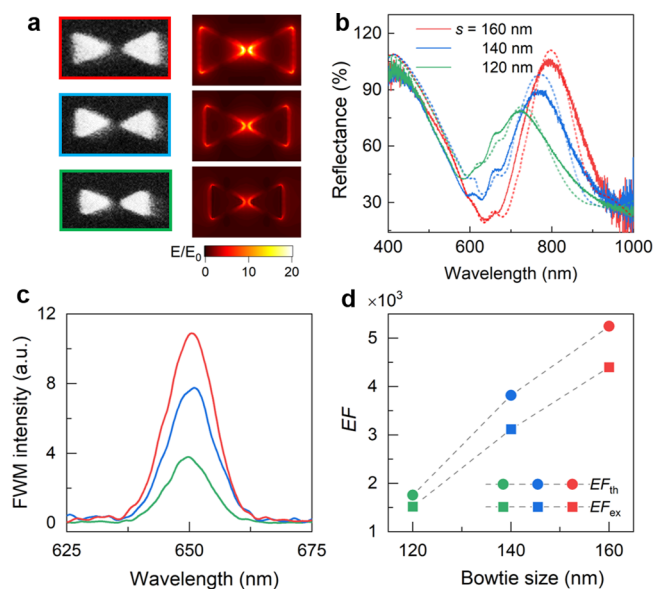


**Figure 4.** FWM enhancement with different plasmonic structure dimensions. (a) SEM images and the simulated electric field at 800 nm of Au bowtie structures with different sizes ( $s = 160, 140,$  and  $120$  nm). (b) Experimental (solid curves) and simulated (dotted curves) relative reflection spectra, (c) experimental FWM spectra, and (d) experimental ( $EF_{\text{ex}}$ ) and theoretical ( $EF_{\text{th}}$ ) enhancement factors of the corresponding MoS<sub>2</sub>-plasmonic structures.

We further experimentally investigate the effect of the structure dimensions on the FWM enhancement in monolayer MoS<sub>2</sub>. The corresponding FWM spectra are measured from the hybrid MoS<sub>2</sub>-plasmonic structures with different nanostructure sizes (Figure 4c). Thus, the experimental ( $EF_{\text{ex}}$ ) and theoretical ( $EF_{\text{th}}$ ) enhancement factors can be calculated, respectively, as shown in Figure 4d. When nanostructure size  $s$  changes from 120 to 160 nm, both the experimental and theoretical enhancement factors increase and show a similar tendency ( $EF_{\text{ex}}$  from 1500 to 4400, and  $EF_{\text{th}}$  from 1750 to 5250). We note that the nanostructure with  $s = 160$  nm gives the highest  $EF_{\text{ex}}$  with on-resonance excitation at 800 nm, while the FWM intensity drops with decreased nanostructure sizes, as expected from the simulation results (Figure 4a). Note that if the size of the nanostructure further increases (i.e.,  $s > 160$  nm), the plasmonic resonance is expected to redshift to a longer wavelength (i.e.,  $> 800$  nm), and thus, the pump laser at 800 nm does not match the plasmonic resonance, leading to the suppression of the FWM enhancement.

**Broadband FWM Enhancement.** The schematic of broadband FWM enhancement is shown in Figure 5a. In our experiments, we fix the pump frequency and change the idler frequency to generate the tunable FWM enhancement in a broad wavelength range. In our case, since the fixed pump frequency matches the plasmonic resonance (i.e.,  $\omega_1 = \omega_{\text{p,L}}$ ), the FWM process is always kept on resonance. Hence, regardless of the tunable idler frequency, the FWM signal will be enhanced over a wide spectral range. To demonstrate the broadband FWM enhancement concept, our pump ( $\hbar\omega_1$ ) is fixed at  $\sim 1.55$  eV (i.e.,  $\lambda_1 = \sim 800$  nm) on resonance with the plasmonic resonance ( $\omega_1 = \omega_{\text{p,L}}$ ), and the idler ( $\hbar\omega_2$ ) changes from  $\sim 0.98$  to 1.41 eV (i.e.,  $\lambda_2 = \sim 1260$  nm  $-$  880 nm), limited by the laser operation range. Both the pump and idler beams are linearly polarized along the  $x$ -axis. As a result, the generated FWM ( $\omega_{\text{FWM}} = 2\omega_1 - \omega_2$ ) is tunable from  $\sim 2.12$  to 1.69 eV

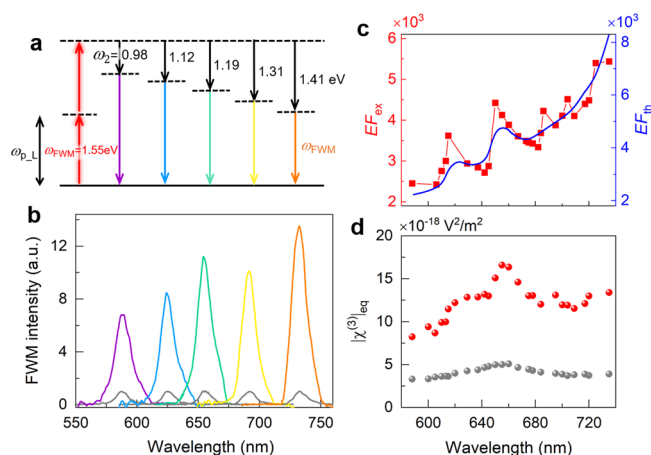


**Figure 5.** Broadband FWM enhancement. (a) Concept of the broadband plasmon-enhanced FWM, where the pump light frequency matches the plasmonic resonance and the idler light frequency changes to generate tunable FWM enhanced in a broad spectral range. (b) Experimental FWM signals at different wavelengths from the hybrid MoS<sub>2</sub>-plasmonic structure (colored curves) and bare MoS<sub>2</sub> (gray curves). The FWM intensity from bare MoS<sub>2</sub> is normalized. (c) Wavelength-dependent experimental (red dots) and theoretical (the blue curve) enhancement factors. (d) Calculated third-order equivalent nonlinear coefficient of FWM in hybrid MoS<sub>2</sub>-plasmonic structure (red dots) and third-order nonlinear coefficient of bare MoS<sub>2</sub> (gray dots).

( $\lambda_{\text{FWM}} = \sim 588\text{--}734\text{ nm}$ ), covering the major part of the visible wavelength region. As shown in Figure 5b, the experimental FWM intensity measured from the hybrid MoS<sub>2</sub>-plasmonic structure is significantly higher than that from the bare MoS<sub>2</sub> over the wide spectral range of 588–734 nm ( $\sim 150\text{ nm}$ ). This result demonstrates that one single plasmonic structure can offer a broadband platform for enhancing FWM and other similar multiwave mixing processes in 2D materials, pushing the previously demonstrated limitation of a narrow spectral range of enhancement such as the cavity-enhanced SHG in 2D materials toward the broadband scheme.<sup>31</sup>

The wavelength-dependent experimental and theoretical enhancement factors are calculated, respectively, as shown in Figure 5c. Over the spectral range, both  $EF_{\text{ex}}$  and  $EF_{\text{th}}$  increase at longer wavelengths. It is mainly because FWM emission is enhanced when the FWM frequency and the idler frequency approach the plasmonic resonance at the wavelength of 800 nm (Figure S7, Supporting Information). Moreover,  $EF_{\text{ex}}$  and  $EF_{\text{th}}$  peaks at around 620 and 660 nm are attributed to the enhanced interaction between MoS<sub>2</sub> and the plasmonic resonance at exciton wavelengths. The detailed discussion is in Figure S7 of the Supporting Information.

On the basis of the measured FWM intensities, the wavelength-dependent third-order nonlinear coefficients  $|\chi^{(3)}|$  of bare MoS<sub>2</sub> and the equivalent nonlinear coefficient  $|\chi^{(3)}|_{\text{eq}}$  of the hybrid MoS<sub>2</sub>-plasmonic structures are calculated from  $\sim 588$  to 734 nm, as shown in Figure 5d. The detailed calculation method is discussed in the Supporting Information. Attributed to the plasmonic enhancement, the equivalent  $|\chi^{(3)}|_{\text{eq}}$  of MoS<sub>2</sub> in the hybrid MoS<sub>2</sub>-plasmonic structure is in the order of  $10^{-17}\text{ m}^2/\text{V}^2$ , which is almost one order of magnitude larger than the previous results and far better than the conventional nonlinear optical materials (such as LiNbO<sub>3</sub>, BBO, Tables 1 and 2 in the Supporting Information).<sup>1</sup> To further improve the FWM enhancement, we can optimize the

nanostructures for improved field enhancement (e.g., shrink the periodicity with a higher filling fraction of nanostructures, narrow down the gap within the bowtie). Besides, we can integrate the hybrid MoS<sub>2</sub>-plasmonic structures into an optical cavity or a waveguide to improve the enhancement.

**Conclusions.** To summarize, we have demonstrated the broadband enhanced nonlinear light–matter interaction in MoS<sub>2</sub> with plasmonic structures. The enhancement factor of FWM up to three orders of magnitude is achieved. The enhancement is attributed to the localized electric field of the pump beam in the hot spot of the plasmonic nanostructures. With the longitudinal plasmonic mode, the plasmonic resonance with the extremely enhanced electric field at the hot spot results in the larger FWM enhancement compared to that of the transverse plasmonic mode. Moreover, a broadband FWM enhancement is realized over 150 nm in the visible spectral range. Our results show that the plasmonic structures can drastically improve the broadband nonlinear light–matter interactions in hybrid MoS<sub>2</sub>-plasmonic structures, boosting the applications of 2D materials for future nonlinear optical devices.

## ■ ASSOCIATED CONTENT

### Supporting Information

The Supporting Information is available free of charge at <https://pubs.acs.org/doi/10.1021/acs.nanolett.1c02381>.

Device fabrication and the characterization of monolayer MoS<sub>2</sub>, nonlinear optical measurement, polarization dependence of FWM, full spectra of different nonlinear optical processes, numerical simulation method, polarization dependence of FWM enhancement, theoretical calculation of enhancement factors, calculation of nonlinear coefficients for FWM signals in MoS<sub>2</sub>, typical third-order nonlinear coefficients reported on 2D layered materials, enhancement factors for nonlinear coefficients of two-dimensional materials in hybrid structures (PDF)

## ■ AUTHOR INFORMATION

### Corresponding Authors

Zhipei Sun – Department of Electronics and Nanoengineering and QTF Centre of Excellence, Department of Applied Physics, Aalto University, Espoo 02150, Finland;

orcid.org/0000-0002-9771-5293; Email: zhipei.sun@aalto.fi

Yunyun Dai – Department of Electronics and Nanoengineering, Aalto University, Espoo 02150, Finland;

orcid.org/0000-0002-1186-1864; Email: yunyun.dai@aalto.fi

### Authors

Yadong Wang – Department of Electronics and Nanoengineering, Aalto University, Espoo 02150, Finland;

orcid.org/0000-0001-8603-3468

Susobhan Das – Department of Electronics and Nanoengineering, Aalto University, Espoo 02150, Finland

Shisheng Li – International Center for Young Scientists (ICYS), National Institute for Materials Science (NIMS), Tsukuba 305-0044, Japan

Hui Xue – Department of Electronics and Nanoengineering, Aalto University, Espoo 02150, Finland; orcid.org/0000-0002-9094-6646

Ahmadi Mohsen – Department of Electronics and Nanoengineering, Aalto University, Espoo 02150, Finland

Complete contact information is available at:  
<https://pubs.acs.org/10.1021/acs.nanolett.1c02381>

### Author Contributions

Y.D. and Z.S. conceived the idea. Y.D. performed the experiments with assistance from Y.W. and S.D. H.X. and A.M. helped the nanostructure fabrication and characterization. S.L. provided the CVD-grown MoS<sub>2</sub> sample. Y.D. analyzed the experimental data. Y.D. and Z.S. wrote the manuscript with contributions from all authors.

### Notes

The authors declare no competing financial interest.

### ACKNOWLEDGMENTS

The authors thank funding from Aalto Centre for Quantum Engineering, Business Finland (A-Photonics), Academy of Finland (Grant Nos. 312297, 312551, 314810, 333982, 336144, and 336818), Academy of Finland Flagship Programme (Grant No. 320167, PREIN), the European Union's Horizon 2020 research and innovation program (Grant No. 820423, S2QUIP; 965124, FEMTOCHIP), the EU H2020-MSCA-RISE-872049 (IPN-Bio), ERC (Grant No. 834742), and Japan Society for the Promotion of Science (JSPS) (Grant No. 19K15399; S19030).

### REFERENCES

- (1) Autere, A.; Jussila, H.; Dai, Y.; Wang, Y.; Lipsanen, H.; Sun, Z. Nonlinear Optics with 2D Layered Materials. *Adv. Mater.* **2018**, *30* (24), e1705963.
- (2) Ferrari, A. C.; Bonaccorso, F.; Fal'ko, V.; Novoselov, K. S.; Roche, S.; Boggild, P.; Borini, S.; Koppens, F. H.; Palermo, V.; Pugno, N.; Garrido, J. A.; Sordan, R.; Bianco, A.; Ballerini, L.; Prato, M.; Lidorikis, E.; Kivioja, J.; Marinelli, C.; Ryhanen, T.; Morpurgo, A.; Coleman, J. N.; Nicolosi, V.; Colombo, L.; Fert, A.; Garcia-Hernandez, M.; Bachtold, A.; Schneider, G. F.; Guinea, F.; Dekker, C.; Barbone, M.; Sun, Z.; Galiotis, C.; Grigorenko, A. N.; Konstantatos, G.; Kis, A.; Katsnelson, M.; Vandersypen, L.; Loiseau, A.; Morandi, V.; Neumaier, D.; Treossi, E.; Pellegrini, V.; Polini, M.; Tredicucci, A.; Williams, G. M.; Hong, B. H.; Ahn, J. H.; Kim, J. M.; Zirath, H.; van Wees, B. J.; van der Zant, H.; Occhipinti, L.; Di Matteo, A.; Kinloch, I. A.; Seyller, T.; Quesnel, E.; Feng, X.; Teo, K.; Rupasinghe, N.; Hakonen, P.; Neil, S. R.; Tannock, Q.; Lofwander, T.; Kinaret, J. Science and Technology Roadmap for Graphene, Related Two-Dimensional Crystals, and Hybrid Systems. *Nanoscale* **2015**, *7* (11), 4598–810.
- (3) Sun, Z.; Hasan, T.; Torrisi, F.; Popa, D.; Privitera, G.; Wang, F.; Bonaccorso, F.; Basko, D. M.; Ferrari, A. C. Graphene mode-locked ultrafast laser. *ACS Nano* **2010**, *4* (2), 803–10.
- (4) Martinez, A.; Sun, Z. Nanotube and graphene saturable absorbers for fibre lasers. *Nat. Photonics* **2013**, *7*, 842.
- (5) Sun, Z.; Martinez, A.; Wang, F. Optical Modulators with 2D Layered Materials. *Nat. Photonics* **2016**, *10* (4), 227–238.
- (6) Gu, T.; Petrone, N.; McMillan, J. F.; van der Zande, A.; Yu, M.; Lo, G. Q.; Kwong, D. L.; Hone, J.; Wong, C. W. Regenerative Oscillation and Four-Wave Mixing in Graphene Optoelectronics. *Nat. Photonics* **2012**, *6* (8), 554–559.
- (7) Hendry, E.; Hale, P. J.; Moger, J.; Savchenko, A. K.; Mikhailov, S. A. Coherent Nonlinear Optical Response of Graphene. *Phys. Rev. Lett.* **2010**, *105* (9), 097401.
- (8) Manzeli, S.; Ovchinnikov, D.; Pasquier, D.; Yazyev, O. V.; Kis, A. 2D Transition Metal Dichalcogenides. *Nat. Rev. Mater.* **2017**, *2* (8), 17033.
- (9) He, K.; Kumar, N.; Zhao, L.; Wang, Z.; Mak, K. F.; Zhao, H.; Shan, J. Tightly Bound Excitons in Monolayer WSe<sub>2</sub>. *Phys. Rev. Lett.* **2014**, *113* (2), 026803.
- (10) Ugeda, M. M.; Bradley, A. J.; Shi, S. F.; da Jornada, F. H.; Zhang, Y.; Qiu, D. Y.; Ruan, W.; Mo, S. K.; Hussain, Z.; Shen, Z. X.; Wang, F.; Louie, S. G.; Crommie, M. F. Giant Bandgap Renormalization and Excitonic Effects in a Monolayer Transition Metal Dichalcogenide Semiconductor. *Nat. Mater.* **2014**, *13* (12), 1091–5.
- (11) Zhang, Y. J.; Oka, T.; Suzuki, R.; Ye, J. T.; Iwasa, Y. Electrically Switchable Chiral Light-Emitting Transistor. *Science* **2014**, *344*, 725–728.
- (12) Sun, Z. Electrically Tuned Nonlinearity. *Nat. Photonics* **2018**, *12*, 383–385.
- (13) Karvonen, L.; Säynätjoki, A.; Huttunen, M. J.; Autere, A.; Amirsolaimani, B.; Li, S.; Norwood, R. A.; Peyghambarian, N.; Lipsanen, H.; Eda, G.; Kieu, K.; Sun, Z. Rapid Visualization of Grain Boundaries in Monolayer MoS<sub>2</sub> by Multiphoton Microscopy. *Nat. Commun.* **2017**, *8* (1), 15714.
- (14) Säynätjoki, A.; Karvonen, L.; Rostami, H.; Autere, A.; Mehravar, S.; Lombardo, A.; Norwood, R. A.; Hasan, T.; Peyghambarian, N.; Lipsanen, H.; Kieu, K.; Ferrari, A. C.; Polini, M.; Sun, Z. Ultra-Strong Nonlinear Optical Processes and Trigonular Warping in MoS<sub>2</sub> Layers. *Nat. Commun.* **2017**, *8* (1), 893.
- (15) Autere, A.; Jussila, H.; Marini, A.; Saavedra, J. R. M.; Dai, Y.; Säynätjoki, A.; Karvonen, L.; Yang, H.; Amirsolaimani, B.; Norwood, R. A.; Peyghambarian, N.; Lipsanen, H.; Kieu, K.; de Abajo, F. J. G.; Sun, Z. Optical Harmonic Generation in Monolayer Group-VI Transition Metal Dichalcogenides. *Phys. Rev. B: Condens. Matter Mater. Phys.* **2018**, *98* (11), 115426.
- (16) Wang, Y.; Ghotbi, M.; Das, S.; Dai, Y.; Li, S.; Hu, X.; Gan, X.; Zhao, J.; Sun, Z. Difference frequency generation in monolayer MoS<sub>2</sub>. *Nanoscale* **2020**, *12*, 19638–19643.
- (17) Kumar, N.; Najmaei, S.; Cui, Q.; Ceballos, F.; Ajayan, P. M.; Lou, J.; Zhao, H. Second-Harmonic Microscopy of Monolayer MoS<sub>2</sub>. *Phys. Rev. B: Condens. Matter Mater. Phys.* **2013**, *87* (16), 161403.
- (18) Li, Y.; Rao, Y.; Mak, K. F.; You, Y.; Wang, S.; Dean, C. R.; Heinz, T. F. Probing Symmetry Properties of Few-Layer MoS<sub>2</sub> and h-BN by Optical Second-Harmonic Generation. *Nano Lett.* **2013**, *13* (7), 3329–33.
- (19) Malard, L. M.; Alencar, T. V.; Barboza, A. P. M.; Mak, K. F.; de Paula, A. M. Observation of Intense Second Harmonic Generation from MoS<sub>2</sub> Atomic Crystals. *Phys. Rev. B: Condens. Matter Mater. Phys.* **2013**, *87* (20), 201401.
- (20) Janisch, C.; Wang, Y.; Ma, D.; Mehta, N.; Elias, A. L.; Perea-Lopez, N.; Terrones, M.; Crespi, V.; Liu, Z. Extraordinary Second Harmonic Generation in Tungsten Disulfide Monolayers. *Sci. Rep.* **2015**, *4*, 5530.
- (21) Li, D.; Xiong, W.; Jiang, L.; Xiao, Z.; Golgir, H. R.; Wang, M.; Huang, X.; Zhou, Y.; Lin, Z.; Song, J.; Ducharme, S.; Jiang, L.; Silvain, J. F.; Lu, Y. Multimodal Nonlinear Optical Imaging of MoS<sub>2</sub> and MoS<sub>2</sub>-Based van der Waals Heterostructures. *ACS Nano* **2016**, *10* (3), 3766–75.
- (22) Balla, N. K.; O'Brien, M.; McEvoy, N.; Duesberg, G. S.; Rigneault, H.; Brasselet, S.; McCloskey, D. Effects of Excitonic Resonance on Second and Third Order Nonlinear Scattering from Few-Layer MoS<sub>2</sub>. *ACS Photonics* **2018**, *5* (4), 1235–1240.
- (23) Wang, G.; Marie, X.; Gerber, I.; Amand, T.; Lagarde, D.; Bouet, L.; Vidal, M.; Balocchi, A.; Urbaszek, B. Giant Enhancement of the Optical Second-Harmonic Emission of WSe<sub>2</sub> Monolayers by Laser Excitation at Exciton Resonances. *Phys. Rev. Lett.* **2015**, *114* (9), 097403.
- (24) Seyler, K. L.; Schaibley, J. R.; Gong, P.; Rivera, P.; Jones, A. M.; Wu, S.; Yan, J.; Mandrus, D. G.; Yao, W.; Xu, X. Electrical Control of Second-Harmonic Generation in a WSe<sub>2</sub> Monolayer Transistor. *Nat. Nanotechnol.* **2015**, *10* (5), 407–11.
- (25) Dai, Y.; Wang, Y.; Das, S.; Xue, H.; Bai, X.; Hulkko, E.; Zhang, G.; Yang, X.; Dai, Q.; Sun, Z. Electrical Control of Interband

Resonant Nonlinear Optics in Monolayer MoS<sub>2</sub>. *ACS Nano* **2020**, *14* (7), 8442–8448.

(26) Yu, H.; Talukdar, D.; Xu, W.; Khurgin, J. B.; Xiong, Q. Charge-Induced Second-Harmonic Generation in Bilayer WSe<sub>2</sub>. *Nano Lett.* **2015**, *15* (8), 5653–7.

(27) Koppens, F. H.; Chang, D. E.; Garcia de Abajo, F. J. Graphene Plasmonics: A Platform for Strong Light-Matter Interactions. *Nano Lett.* **2011**, *11* (8), 3370–7.

(28) Cox, J. D.; Marini, A.; de Abajo, F. J. Plasmon-Assisted High-Harmonic Generation in Graphene. *Nat. Commun.* **2017**, *8*, 14380.

(29) Eda, G.; Maier, S. A. Two-Dimensional Crystals: Managing Light for Optoelectronics. *ACS Nano* **2013**, *7* (7), 5660–5665.

(30) Guo, Q.; Ou, Z.; Tang, J.; Zhang, J.; Lu, F.; Wu, K.; Zhang, D.; Zhang, S.; Xu, H. Efficient Frequency Mixing of Guided Surface Waves by Atomically Thin Nonlinear Crystals. *Nano Lett.* **2020**, *20* (11), 7956–7963.

(31) Gan, X. T.; Zhao, C. Y.; Hu, S. Q.; Wang, T.; Song, Y.; Li, J.; Zhao, Q. H.; Jie, W. Q.; Zhao, J. L. Microwatts Continuous-Wave Pumped Second Harmonic Generation in Few- and Mono-Layer GaSe. *Light: Sci. Appl.* **2018**, *7*, 17126.

(32) Uddin, S.; Debnath, P. C.; Park, K.; Song, Y. W. Nonlinear Black Phosphorus for Ultrafast Optical Switching. *Sci. Rep.* **2017**, *7*, 43371.

(33) Shi, J.; Liang, W.-Y.; Raja, S. S.; Sang, Y.; Zhang, X.-Q.; Chen, C.-A.; Wang, Y.; Yang, X.; Lee, Y.-H.; Ahn, H.; Gwo, S. Plasmonic Enhancement and Manipulation of Optical Nonlinearity in Monolayer Tungsten Disulfide. *Laser Photonics Rev.* **2018**, *12* (10), 1800188.

(34) Wang, Z.; Dong, Z.; Zhu, H.; Jin, L.; Chiu, M. H.; Li, L. J.; Xu, Q. H.; Eda, G.; Maier, S. A.; Wee, A. T. S.; Qiu, C. W.; Yang, J. K. W. Selectively Plasmon-Enhanced Second-Harmonic Generation from Monolayer Tungsten Diselenide on Flexible Substrates. *ACS Nano* **2018**, *12* (2), 1859–1867.

(35) Renger, J.; Quidant, R.; van Hulst, N.; Novotny, L. Surface-Enhanced Nonlinear Four-Wave Mixing. *Phys. Rev. Lett.* **2010**, *104* (4), 046803.

(36) Palomba, S.; Novotny, L. Nonlinear Excitation of Surface Plasmon Polaritons by Four-Wave Mixing. *Phys. Rev. Lett.* **2008**, *101* (5), 056802.

(37) Zhang, Y.; Wen, F.; Zhen, Y. R.; Nordlander, P.; Halas, N. J. Coherent Fano Resonances in a Plasmonic Nanocluster Enhance Optical Four-Wave Mixing. *Proc. Natl. Acad. Sci. U. S. A.* **2013**, *110* (23), 9215–9.

(38) Wen, X.; Xu, W.; Zhao, W.; Khurgin, J. B.; Xiong, Q. Plasmonic Hot Carriers-Controlled Second Harmonic Generation in WSe<sub>2</sub> Bilayers. *Nano Lett.* **2018**, *18* (3), 1686–1692.

(39) Chen, W.; Zhao, J.; Zhang, J.; Gu, L.; Yang, Z.; Li, X.; Yu, H.; Zhu, X.; Yang, R.; Shi, D.; Lin, X.; Guo, J.; Bai, X.; Zhang, G. Oxygen-Assisted Chemical Vapor Deposition Growth of Large Single-Crystal and High-Quality Monolayer MoS<sub>2</sub>. *J. Am. Chem. Soc.* **2015**, *137* (50), 15632–5.

(40) Guo, X.; Zou, C.-L.; Tang, H. X. Second-Harmonic Generation in Aluminum Nitride Microrings with 2500%/W Conversion Efficiency. *Optica* **2016**, *3* (10), 1126–1131.

(41) Zhu, X.; Vannahme, C.; Hojlund-Nielsen, E.; Mortensen, N. A.; Kristensen, A. Plasmonic Colour Laser Printing. *Nat. Nanotechnol.* **2016**, *11* (4), 325–9.

(42) Wang, Z.; Dong, Z.; Gu, Y.; Chang, Y. H.; Zhang, L.; Li, L. J.; Zhao, W.; Eda, G.; Zhang, W.; Grinblat, G.; Maier, S. A.; Yang, J. K.; Qiu, C. W.; Wee, A. T. Giant Photoluminescence Enhancement in Tungsten-Diselenide-Gold Plasmonic Hybrid Structures. *Nat. Commun.* **2016**, *7*, 11283.

(43) Rechberger, W.; Hohenau, A.; Leitner, A.; Krenn, J. R.; Lamprecht, B.; Aussenegg, F. R. Optical Properties of Two Interacting Gold Nanoparticles. *Opt. Commun.* **2003**, *220* (1–3), 137–141.

(44) Le, K. Q.; Alu, A.; Bai, J. Multiple Fano Interferences in a Plasmonic Metamolecule Consisting of Asymmetric Metallic Nanodimers. *J. Appl. Phys.* **2015**, *120* (117), 023118.